



Antarctic subglacial conditions inferred from a hybrid ice sheet/ice stream model

Frank Pattyn

Laboratoire de Glaciologie, Département des Sciences de la Terre et de l'Environnement, CP160/03, Université Libre de Bruxelles, Av. F.D. Roosevelt 50, B-1050 Brussels, Belgium

ARTICLE INFO

Article history:

Received 15 October 2009

Received in revised form 9 April 2010

Accepted 12 April 2010

Available online 18 May 2010

Editor: M.L. Delaney

Keywords:

Antarctic ice sheet
numerical modeling
subglacial temperature
geothermal heat-flow
basal melting
ice sheet age

ABSTRACT

Subglacial conditions of large polar ice sheets remain poorly understood, despite recent advances in satellite observation. Major uncertainties related to basal conditions, such as the temperature field, are due to an insufficient knowledge of geothermal heat flow. Here, a hybrid method is presented that combines numerical modeling of the ice sheet thermodynamics with a priori information using a simple assimilation technique. Additional data are essentially vertical temperature profiles measured in the ice sheet at selected spots, as well as the distribution of subglacial lakes. In this way, geothermal heat-flow datasets are improved to yield calculated temperatures in accord with observations in areas where information is available. Results of the sensitivity experiments show that 55% of the grounded part of the Antarctic ice sheet is at pressure melting point. Calculated basal melt rates are approximately 65 Gt year^{-1} , which is 3% of the total surface accumulation. Although these sensitivity experiments exhibit small variations in basal melt rates, the impact on the ice age of basal layers is quite important. In areas that are characterized by relatively low melt rates, this may lead to standard deviations up to 50% (in a model run over a period of 10^6 years). Subglacial water flow is concentrated underneath the large outlet glaciers of Antarctica. The larger subglacial lakes are perched at the head of these subglacial water systems. An exception, however, is the lake system of the Recovery Ice Stream Catchment, that receives a substantial amount of subglacial melt water from the upstream catchment.

© 2010 Elsevier B.V. All rights reserved.

1. Introduction

Although a great deal is known about the surface of the Antarctic ice sheet through on-site measurements and satellite observations, basal conditions (temperature and hydrology) are poorly understood. Nevertheless, basal conditions govern to a large extent the dynamical behavior of ice masses. Underneath present-day ice streams and outlet glaciers of Antarctica and Greenland, water and deformable wet sediments lubricate the base, hence facilitating fast ice flow. Unexpected accelerations in outlet glaciers of the Greenland and the Antarctic ice sheets occur, probably related to sudden variations in subglacial water presence. Therefore, a key uncertainty remains the interaction between the ice and its underlying bed, which controls how basal velocity will change as ice sheet stresses evolve. An increase in the contribution of ice sheets to global sea level due to acceleration of these ice streams is to be expected (Bell, 2008).

Knowledge of basal ice sheet conditions is also essential in the quest for oldest ice, which occurs where basal ice layers are frozen to the bed. Obvious places to look for are the deepest parts of the ice sheet, where ice is thick, and accumulation rates are low. However, a thick ice cover insulates very well and keeps the geothermal heat from escaping to the surface. Many deep ice core drill sites in Antarctica have basal ice close or at the pressure melting point, such as at Vostok,

EPICA Dome C, EPICA DML and Dome Fuji (Salamatin et al., 1994; Augustin et al., 2007). Furthermore, we know that more than 280 subglacial lakes exist under the Antarctic ice sheet, which implies that large portions of the bedrock should be at pressure melting point (e.g. Bell, 2008; Smith et al., 2009)). These subglacial lakes occur at and may be linked to the upglacier limit of rapid ice flow (Bell et al., 2007). However, release of stored lake water in outburst floods (Fricker et al., 2007; Smith et al., 2009) does not seem to have major ice-flow effects, although the process of water exchange between subglacial lakes may be a widespread phenomenon, as model studies suggest (Pattyn, 2008).

Geophysical exploration is essential but cannot sample everything (Alley et al., 2008). Direct measurements of basal temperature are therefore limited to a number of selected boreholes through the ice. A few ice core and subglacial sediment samples have been retrieved in central parts of the ice sheet (Christoffersen and Tulaczyk, 2003), but these remain fragmentary. Thence, we have to rely on other techniques, such as ice sheet modeling, to catch a glimpse of the sub-ice environment.

Several authors tried to elucidate basal temperature conditions of the ice sheet. One of the earlier estimates is due to Zotikov (1963), showing the central parts of the Antarctic ice sheet at pressure melting point, an area of hundreds of thousands of square kilometers, incorporating the sites of Vostok, Byrd and Amundsen–Scott Stations. Although the physics were well understood at that time, the lack of detailed measurements on surface topography and bedrock

E-mail address: fpattyn@ulb.ac.be.

prevented a more rigorous approach and the basal temperature field remained rather schematic. It is only with the advent of satellite altimetry, revealing detailed surface topography (Liu et al., 1999) and more comprehensive bedrock elevation datasets (Drewry, 1983; Lythe and Vaughan, 2001) that better estimates could be produced (Pollard et al., 2005; Siegert et al., 2005b; Huybrechts, 2006; Llubes et al., 2006). However, the quality of the basal temperature distribution remains highly dependent on the distribution of geothermal heat flux.

In this paper, we use a hybrid technique, combining a priori information (such as ice core data, on-site measurements and subglacial lake distributions), high resolution datasets of surface and bed topography, accumulation (and decadal variations in accumulation), surface temperature, geothermal heat flow (and heat-flow anomalies) with a merged ice sheet/ice stream model in order to calculate present-day temperature and age fields of the Antarctic ice sheet. A sensitivity analysis is also carried out to evaluate uncertainties of the derived temperature and age fields.

2. Model description

Previous basal temperature assessments of the Antarctic ice sheet are based on time dependent numerical ice sheet modeling, where either a steady-state simulation is performed under present-day climate conditions (Siegert et al., 2005b), or the ice sheet is forced over a number of glacial-interglacial cycles by the climatic record until present, to yield a realistic ice sheet temperature field (Huybrechts, 2002). The latter type of simulation therefore includes transient effects, because the temperature field reacts slowly on long-term climate variability. However, in both cases the modeled ice sheet surface topography may differ quite a lot from present-day observed topography by several hundreds of meters, since it is a free surface condition. Modeled temperature profiles may therefore differ from measured temperature profiles. For the purpose of this assessment, we consider the present ice sheet topography and its temperature distribution in steady state, and adjust free parameters in such a way to keep modeled temperature profiles in agreement with observed profiles at the different drill sites in Antarctica.

2.1. Temperature field

The thermodynamic equation for the temperature distribution in an ice mass is given by

$$\frac{\partial T}{\partial t} = \nabla \left(\frac{k}{\rho c} \nabla T \right) - \mathbf{v} \cdot \nabla T - \frac{2}{\rho c} \dot{\epsilon} \sigma, \quad (1)$$

where T is the ice temperature (K), $k = 3.101 \times 10^8 \exp(-0.0057 T) \text{ J m}^{-1} \text{ K}^{-1} \text{ year}^{-1}$ is the thermal conductivity (Ritz, 1987), $c = 2115.3 + 7.79293 (T - 273.15) \text{ J kg}^{-1} \text{ K}^{-1}$ is the heat capacity (Pounder, 1965), and $\mathbf{v} = (v_x, v_y, v_z)$ is the three-dimensional ice velocity vector (m year^{-1}). The last term on the right-hand side represents internal heating rate per unit volume (Pattyn, 2003), where $\dot{\epsilon}$ and σ are effective strain rate and effective shear stress, respectively. Horizontal diffusion is neglected, and the temperature field is considered to be in steady state ($\frac{\partial T}{\partial t} = 0$). Since it is convenient to work in normalized coordinates, a sigma coordinate system is introduced, i.e. $\zeta = (s - z)/H$, where s and H are the ice sheet surface and ice thickness, respectively, and z is the vertical axis positive pointing upwards, so that for $z = s$, $\zeta = 0$ and for $z = b$, $\zeta = 1$. The thermodynamic Eq. (1) is then reformulated as

$$\begin{aligned} \frac{\partial T}{\partial \zeta} \left(a_x v_x + a_y v_y - \frac{v_z}{H} \right) - \frac{k}{\rho c H^2} \frac{\partial^2 T}{\partial \zeta^2} \\ = \frac{2}{\rho c} \dot{\epsilon} \sigma - v_x \frac{\partial T}{\partial x} - v_y \frac{\partial T}{\partial y}, \end{aligned} \quad (2)$$

where

$$a_{x_i} = \frac{1}{H} \left(\frac{\partial s}{\partial x_i} - \zeta \frac{\partial H}{\partial x_i} \right), \quad (3)$$

where $x_i = (x, y)$. The vertical velocity v_z at the surface is negative in case of accumulation. Considering the most important heat source from vertical shearing, internal heating may be simplified to (Huybrechts, 1992):

$$\frac{2}{\rho c} \dot{\epsilon} \sigma \approx \frac{g \zeta}{c} \frac{\partial \mathbf{v}_H}{\partial \zeta} \nabla_H s, \quad (4)$$

where g is the gravitational constant and $\mathbf{v}_H = (v_x, v_y)$. Boundary conditions for (2) are the surface temperature T_s and a basal temperature gradient, based on the geothermal heat flux:

$$\frac{\partial T}{\partial \zeta} \Big|_b = \frac{H}{k} (G + \tau_b \mathbf{v}_b), \quad (5)$$

where G is the geothermal heat flux entering the base of the ice sheet and the second term on the right-hand side of (5) heat produced due to basal sliding. τ_b is the basal shear stress, and can be defined as $\tau_b = -\rho g H \nabla_H s$. Whenever pressure melting point is reached, the temperature in the ice is kept at this value:

$$T_{\text{pmp}} = T_0 - \gamma H \zeta, \quad (6)$$

where $T_0 = 273.15 \text{ K}$ and $\gamma = 8.7 \times 10^{-4} \text{ K m}^{-1}$.

In ice shelves, temperature is determined analytically, considering the accumulation at the surface balanced by basal melting underneath an ice shelf and with only vertical diffusion and advection into play, the vertical temperature profile is determined as follows (Holland and Jenkins, 1999)

$$T(\zeta) = \frac{(T_s - T_b) \exp(\beta_1) + T_b - T_s \exp(\beta_2)}{1 - \exp(\beta_2)}, \quad (7)$$

where $\beta_1 = -\rho c v_\zeta(0) H \zeta / k$ and $\beta_2 = -\rho c v_\zeta(0) H / k$, and where $T_b = -2 \text{ }^\circ\text{C}$ is the temperature at the ice/ocean interface.

2.2. Velocity field

Ice sheet velocities are obtained from balance fluxes. The balance assumption is that the mass of ice flowing out of any area within the horizontal domain (x, y) exactly equals the sum of the inflow and the ice accumulated over the area (Budd and Warner, 1996; Fricker et al., 2000; Le Brocq et al., 2006),

$$\nabla_H \mathbf{q}_s = a, \quad (8)$$

with

$$\mathbf{q}_s = -H \int_1^0 v_H(\zeta') d\zeta', \quad (9)$$

and where a is the accumulation rate (m year^{-1} ice equivalent). Integrating (8) over the whole surface of the ice sheet, starting at the ice divides, one obtains the vertically averaged horizontal balance velocities $\bar{\mathbf{v}}_H = (\bar{v}_x, \bar{v}_y)$. This is done with the GDS-Warner algorithm, based on Budd and Warner (1996) and modified by using the gravitational driving stress (GDS) as a guidance of the ice flow instead of the local surface slope (Le Brocq et al., 2006). The GDS is calculated over horizontal distances of 5 times the local ice thickness to account for longitudinal averaging on the local flow (Kamb and Echelmeyer,

1986; Le Brocq et al., 2006). The three-dimensional horizontal velocities are then determined from the shallow-ice approximation (Hutter, 1983), by

$$\mathbf{v}_H(x, y, \zeta) = \left(\frac{n+2}{n+1} \bar{\mathbf{v}}_H - \mathbf{v}_b \right) \left(1 - \zeta^{n+1} \right) + \mathbf{v}_b, \quad (10)$$

where $n=3$ is the flow exponent from Glen's flow law. However, (10) is only valid for an isothermal ice sheet. Parrenin et al. (2004) provide a similar formulation for the horizontal velocity field along a flowline between the ice divide and Subglacial Lake Vostok. To account for temperature effects, hence softening of the ice at the bottom due to higher temperatures, they let the exponent vary between $n=5$ (at the divide) and $n=10$ elsewhere along the flowline. Further sensitivities were carried out with lower values of n , leading to small variations in the thinning function (Parrenin et al., 2004). Considering the ice sheet isothermal may lead to an underestimation of heat production and vertical advection, albeit that both have an opposite effect on the basal temperature.

Basal sliding may occur in the grounded ice sheet whenever pressure melting point is reached (the treatment for subglacial lakes, ice streams and ice shelves is explained below). A Weertman sliding law is introduced with a correction to allow for basal sliding at subfreezing temperatures over a range of $\psi=1$ K (Hindmarsh and Le Meur, 2001).

$$\mathbf{v}_b = A_s \frac{\tau_b^m}{\rho g H} \exp \left[\psi^{-1} (T_b - T_{\text{pmp}}) \right], \quad (11)$$

where $A_s=5 \times 10^{-7}$ m Pa $^{1-m}$ year $^{-1}$ is a sliding parameter, $\mathbf{v}_b=(v_x(b), v_y(b))$ and $m=3$.

Over large subglacial lakes and in ice streams, the shallow-ice approximation does not apply anymore and balance velocities are corrected using an ice stream/ice shelf model similar to MacAyeal (1989). The velocity field is not locally defined, but depends on horizontal stress gradients (membrane stresses; Hindmarsh, 2006). Velocities are independent of ζ , so that the depth averaged velocity is obtained through solution of the following set of equations

$$\frac{\partial}{\partial x} \left[2\nu H \left(2 \frac{\partial v_x}{\partial x} + \frac{\partial v_y}{\partial y} \right) \right] + \frac{\partial}{\partial y} \left[\nu H \left(\frac{\partial v_x}{\partial y} + \frac{\partial v_y}{\partial x} \right) \right] - \beta^2 v_y = \rho g H \frac{\partial s}{\partial x} \quad (12)$$

$$\frac{\partial}{\partial y} \left[2\nu H \left(2 \frac{\partial v_y}{\partial y} + \frac{\partial v_x}{\partial x} \right) \right] + \frac{\partial}{\partial x} \left[\nu H \left(\frac{\partial v_x}{\partial y} + \frac{\partial v_y}{\partial x} \right) \right] - \beta^2 v_x = \rho g H \frac{\partial s}{\partial y}, \quad (13)$$

where

$$v = \frac{A^{-1/n}}{2 \left[\left(\frac{\partial v_x}{\partial x} \right)^2 + \left(\frac{\partial v_y}{\partial y} \right)^2 + \frac{1}{4} \left(\frac{\partial v_x}{\partial y} + \frac{\partial v_y}{\partial x} \right)^2 + \frac{\partial v_x}{\partial x} \frac{\partial v_y}{\partial y} \right]^{\frac{n-1}{2n}}} \quad (14)$$

is the effective viscosity, A the flow-rate factor in Glen's flow law (taken as 5×10^{-19} Pa $^{-n}$ year $^{-1}$), and β^2 is a basal friction parameter taken as $\beta^2=250$ Pa year m $^{-1}$ for ice streams and $\beta^2=0$ ice shelves or subglacial lakes (Pattyn, 2003; Pattyn et al., 2006; Pattyn, 2008). The numerical procedure to correct the velocity field is explained in 2.3. The correction of balance velocities across large subglacial lakes with this ice stream model is essential to get the flow direction correct. For instance, the surface slope across Subglacial Lake Vostok is from north to south (hence the velocity direction obtained from balance fluxes as well), while the observed movement of the ice and

the motion calculated with the stream model is from west to east (Studinger et al., 2003; Pattyn et al., 2004). For coastal ice shelves, a seaward boundary conditions is given by (Joughin et al., 2009):

$$2\nu H \left(2 \frac{\partial v_x}{\partial x} + \frac{\partial v_y}{\partial y} \right) \mathbf{n}_x + \nu H \left(\frac{\partial v_x}{\partial y} + \frac{\partial v_y}{\partial x} \right) \mathbf{n}_y = \rho g \frac{H_s}{2} \mathbf{n}_x \quad (15)$$

$$2\nu H \left(2 \frac{\partial v_y}{\partial y} + \frac{\partial v_x}{\partial x} \right) \mathbf{n}_y + \nu H \left(\frac{\partial v_x}{\partial y} + \frac{\partial v_y}{\partial x} \right) \mathbf{n}_x = \rho g \frac{H_s}{2} \mathbf{n}_y. \quad (16)$$

Subglacial lakes in ice streams (Fricker et al., 2007; Fricker and Scambos, 2009) are not accounted for explicitly, as the same model is applied anyway. The onset of ice stream flow was taken as 100 m year $^{-1}$ (Bindschadler et al., 2001).

The vertical velocity field is derived from mass conservation combined with the incompressibility condition for ice. Given an ice sheet in steady state, a simple analytical expression can be obtained, based on the horizontal balance velocities (Hindmarsh, 1999; Hindmarsh et al., 2009):

$$v_\zeta(x, y, \zeta) = - \left[\frac{\zeta^{n+2} - 1 + (n+2)(1-\zeta)}{n+1} \right] a - m + \mathbf{v}_H \nabla b + (1-\zeta) \mathbf{v}_H \nabla H, \quad (17)$$

where m is the basal melting rate, computed as follows

$$m = \left(\frac{\partial T}{\partial \zeta} \Big|_b - \frac{\partial T}{\partial \zeta} \Big|_c \right) \frac{k}{\rho L H}. \quad (18)$$

Subscript c denotes the correction of the basal temperature gradient whenever pressure melting point (6) is reached, and where L is the specific latent heat of fusion (3.35×10^5 J kg $^{-1}$).

2.3. Numerical solution

The model is implemented on a numerical grid of 5×5 km in the horizontal with 21 unevenly distributed layers in the vertical (smallest grid spacing $\Delta\zeta=0.015$ closest to the bed). A mask is used to identify whether the ice sheet is grounded or floating and where subglacial lakes occur. During a first iteration the balance velocity field is calculated. Basal velocities in the grounded ice sheet are determined from (11). The complete horizontal velocity field in the grounded ice sheet is then determined from balance and basal velocities using (10). Subsequently, the ice stream model is applied to calculate velocities across subglacial lakes, in ice streams and ice shelves using the balance velocities as boundary conditions (where applied). The stream-lake region is considered to be in steady state as the geometry of the system is not changing (diagnostic velocity field). Since the calculation of velocities across the lake alters the flux downstream, the balance flux downstream is calculated iteratively.

The temperature field calculation is slightly more complicated, as basal temperatures influence the basal sliding and melt, which, in turn influences the vertical velocities. Furthermore, both strain heating and advection rely on the velocity field. As a first guess, the temperature field is determined using the originally-determined velocity field without melting. Subsequently, both horizontal and vertical velocities are updated as basal melting gets introduced, until convergence is reached. This generally occurs after 5 to 10 iterations.

3. Input data

3.1. Global Antarctic data sets

Surface topography is based on satellite radar altimetry data from the geodetic phase of the ERS-1 satellite mission and combined with laser altimeter measurements from the Geosciences Laser Altimeter System on board ICESat (Fig. 1; Bamber et al., 2009). The original dataset was resampled at 5 km resolution.

Bedrock topography is based on the BEDMAP database (Lythe and Vaughan, 2001), but regionally improved for areas such as Dronning Maud Land (Huybrechts et al., 2000), Subglacial Lake Vostok (Studinger et al., 2003), and the Dome Fuji region (Fujita et al., 1999; Watanabe et al., 2003, S. Fujita, personal communication, 2006).

Surface mass balance is obtained from van de Berg et al. (2006) and van den Broeke et al. (2006), based on the output of a regional atmospheric climate model for the period 1980 to 2004 and calibrated using observed mass balance rates. A regional enhancement was done for the Subglacial Lake Vostok region with long-term accumulation data from MacGregor et al. (2009). For the purpose of sensitivity testing, surface accumulation rates were perturbed using decadal Antarctic snowfall anomalies for the period 1985–1994 and 1995–2004 (Monaghan et al., 2006).

Surface temperatures are due to van den Broeke (2008), based on a combined regional climate model, calibrated with observed 10 m ice temperatures.

For the geothermal heat flow (GHF) we rely on two existing datasets. The first one uses a global seismic model of the crust and the

upper mantle to guide the extrapolation of existing heat-flow measurements to regions where such measurements are rare or absent (Shapiro and Ritzwoller, 2004). In general, highest GHF values are found in West Antarctica, while the East Antarctic craton is characterized by very low GHF values (corresponding to the old rock age). The second GHF database stems from satellite magnetic measurements (Fox-Maule et al., 2005). Values of GHF are in the same range as Shapiro and Ritzwoller (2004), but the spatial variability is contrasting. Heat-flow measurements according to Fox-Maule et al. (2005) are also significantly higher in East Antarctica than those from Shapiro and Ritzwoller (2004). Another way of obtaining approximate values of GHF is to rely on orogen distributions (Pollard et al., 2005; Llubes et al., 2006). Following Pollard et al. (2005), a third GHF dataset was added, with West Antarctic = 70, Transantarctic = 60, Mawson craton = 41, and the remaining East Antarctic = 55 mW m⁻². The regional pattern of this GHF matches closest with Shapiro and Ritzwoller (2004). For the purpose of the sensitivity experiments, all three datasets were used, either apart or as a combination of two or three. Two more experiments were carried out with a spatially uniform GHF of 42 and 54 mW m⁻², corresponding to a low and a high end member in the analysis, respectively. Both values are common in modeling studies of the Antarctic ice sheet (Hansen and Greve, 1996; Ritz et al., 2001; Huybrechts, 2002).

3.2. Data calibration with ice core data

Direct measurements of GHF are very rare, and are usually obtained from temperature measurements in boreholes of deep ice

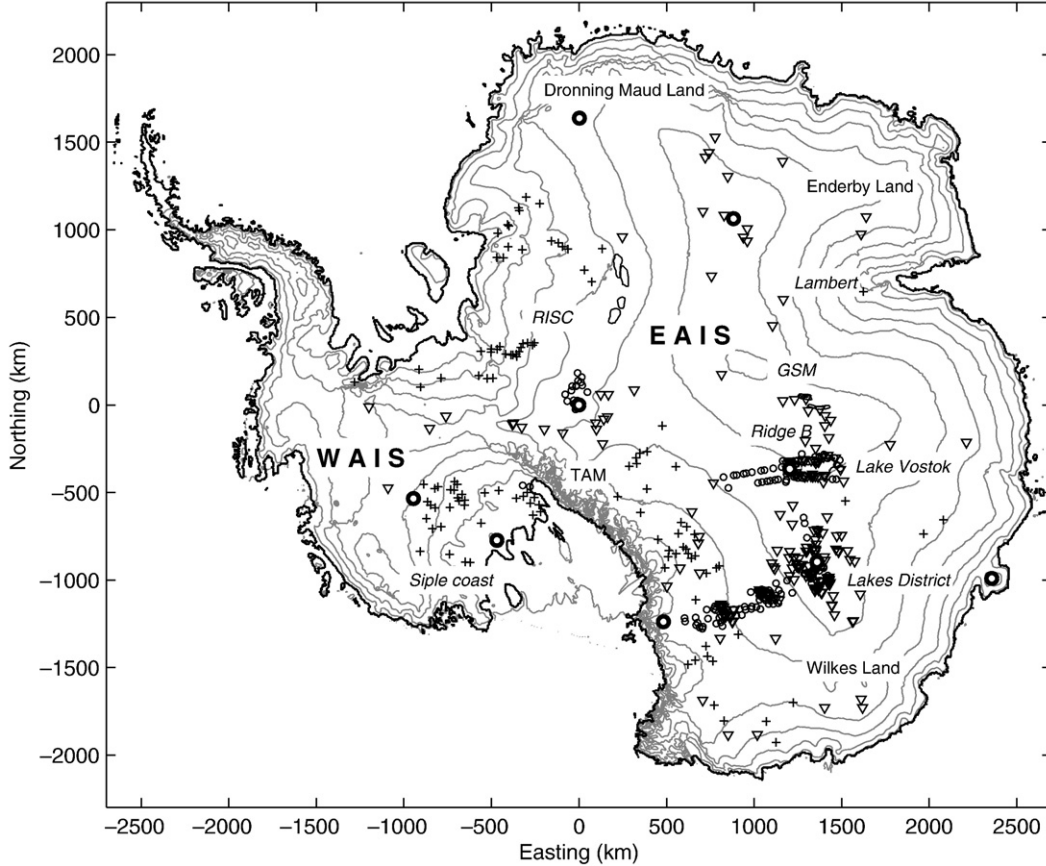


Fig. 1. Surface topography (Bamber et al., 2009) of the Antarctic ice sheet with RES identified large subglacial lakes (black lines), definite (∇) subglacial lakes (Siegent et al., 2005a; Carter et al., 2007; Popov and Maslov, 2007), fuzzy (\circ) lakes (Carter et al., 2007) and active (+) lakes (Smith et al., 2009). The large dots show the position of the deep drill sites where the temperature profile is measured. The present-day grounding line is shown by a black line. WAIS = West Antarctic Ice Sheet; EAIS = East Antarctic Ice Sheet; TAM = Transantarctic Mountains; RISC = Recovery Ice Stream Catchment; GSM = Gamburtsev Subglacial Mountains.

core drillings. Basal temperature gradients in observed temperature profiles of deep boreholes were compared with GHF data from both datasets, and show rather large discrepancies. Therefore, all datasets were corrected using observed basal temperature gradients, surface temperature and accumulation rates, in such a way that modeled temperature profiles match as close as possible the observed ones. In reality, there always remains a discrepancy, since only free parameters (such as surface accumulation, surface temperature and geothermal heat flow) are corrected for. These will essentially control vertical diffusion and advection. Since horizontal advection is controlled by calculated velocities (according to the coupled balance/ice stream models), slight deviations from observed temperatures may persist.

Such corrections are made for sites where temperature profiles are at hand, such as Byrd (Gow et al., 1968), Taylor Dome (G. Clow and E. Waddington, personal communication 2008), Siple Dome (MacGregor et al., 2007), Law Dome (Dahl-Jensen et al., 1999; van Ommen et al., 1999), Vostok (Salamatin et al., 1994; Parrenin et al., 2004), South Pole (Price et al., 2002), Dome Fuji (Fujii et al., 2002; Hondoh et al., 2002), EPICA Dome C (Parrenin et al., 2007, C. Ritz, personal communication 2008), and EPICA DML (Ruth et al., 2007). The applied method consists of determining the difference between observed (X_o) and corresponding database values and to adapt a Gaussian function for a sufficient large influence area. For a variable in the database X (either surface accumulation, surface temperature or geothermal heat flux), its corrected value X_c based on an observation X_o is obtained by

$$X_c(x, y) = X + [X_o - X] \exp \left[-\frac{x^2 + y^2}{\sigma^2} \right], \quad (19)$$

where σ is set to 200 km around the site for which the observation exists, and (x, y) is the horizontal distance from this observed position (0,0). As such, by tuning GHF (constraining the vertical temperature gradient) and surface mass balance (constraining vertical advection), the difference between modeled and observed temperature profiles is less than 2 K. The remaining difference is still due to horizontal advection, which is a model output, as well as past changes in surface temperature that were not taken into account explicitly.

3.3. Data calibration with subglacial lakes

Numerous subglacial lakes are identified from radio-echo sounding (Fig. 1), i.e. 145 from an inventory by Siegert et al. (2005a), and more than 130 added since (Bell et al., 2006, 2007; Carter et al., 2007; Popov and Masolov, 2007; Smith et al., 2009). Subglacial lakes are usually identified from radio-echo sounding (RES) and characterized by a strong basal reflector and a constant echo strength (corroborating a smooth surface). They are brighter than their surroundings by at least 2 dB (relatively bright) and both are consistently reflective (specular) and therefore called *definite* lakes (Carter et al., 2007). The larger ones are characterized by a flat surface compared to the surroundings with a slope around ten times, and in the opposite direction to, the lake surface slope (Siegert et al., 2005a). The ice column above such a subglacial lake is therefore in hydrostatic equilibrium. Fuzzy lakes are defined by high absolute and relative reflection coefficients, but are not specular (Carter et al., 2007). They are interpreted to correspond to saturated basal sediments (Peters et al., 2005; Carter et al., 2007).

From NASA's Ice, Cloud and land Elevation Satellite (ICESat) laser altimetry data, Fricker et al. (2007) determined active subglacial lakes. These are spots where a rapid lowering of the ice surface is detected, followed by a gradual increase of surface elevation. This phenomenon has been interpreted as a sudden drainage of a subglacial lake (over a period of several months), followed by lake filling with subglacial

water from upstream (Fricker et al., 2007; Fricker and Scambos, 2009). Since then, more than 120 active lakes have been identified from ICESat data (Smith et al., 2009).

These three types of lakes are used to constrain the GHF datasets, considering these areas to be at pressure melting point. As such, the minimum GHF needed to reach pressure melting point at the ice/bedrock interface can be determined analytically (Hindmarsh, 1999; Siegert, 2000). Using the simplified model of Hindmarsh (1999), the minimum heat flow needed to reach pressure melting point is

$$G_{min} = \frac{k(T_0 - \gamma H - T_s)}{H(W(1) - W(0))}, \quad (20)$$

where

$$W(\xi) = \int_1^\xi \exp \left(\frac{\lambda(\zeta') H a p c}{k} \right) d\zeta', \quad (21)$$

and where

$$\lambda(\xi) = \frac{\xi^{n+3} - 1}{(n+1)(n+3)} - \frac{(n+2)(\xi^2 - 1)}{2(n+1)} + \xi - 1. \quad (22)$$

The value for G_{min} is a minimum value, which means that if at that spot the database contains a higher value, the latter is retained. Spatial corrections are subsequently applied using the Gaussian function defined in (19). For lakes at subgrid dimensions the correction is also applied, as this situation can be considered as a mixed grid point. The calculation is done with the thickness corresponding to the grid cell thickness. An example of a corrected GHF dataset (based on a combination of Shapiro and Ritzwoller (2004) and Pollard et al. (2005)) is given in Fig. 2. In general, this combined dataset is characterized by low GHF values in East Antarctica compared to West Antarctica. The lowest GHF is found in the Lakes District, despite the abundance of subglacial lakes in this area. Low accumulation rates and thick ice, reducing vertical advection and guaranteeing increased insulation, respectively, require only low values of GHF to reach pressure melting point. This is in accordance with the GHF datasets of Shapiro and Ritzwoller (2004) and Pollard et al. (2005). A suspiciously hot spot is found in the Recovery ice stream catchment. However, this may be an artifact as ice thickness is poorly known in this area.

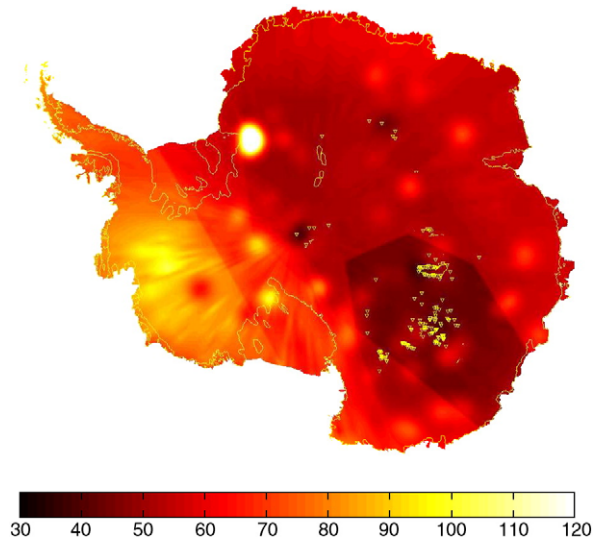


Fig. 2. Geothermal heat flow (GHF) based on a combination of Shapiro and Ritzwoller (2004) and Pollard et al. (2005) and corrected for basal temperature gradients from ice cores as well as the distribution of different subglacial lake types using (19)–(22).

Nevertheless, this spot has only a limited effect on the determination of temperatures and basal melting rates. The mean GHF value of all used datasets and their corrections is $59 \pm 5.7 \text{ mW m}^{-2}$. This value is of the same order of magnitude as the spatially uniform GHF used by others (Ritz et al., 2001; Huybrechts, 2002; Siegert et al., 2005b). However, as will be shown below, the spatial distribution of GHF is a crucial factor in the determination of the temperature field.

4. Sensitivity experiments

4.1. Experimental setup

Major sources of uncertainty in the determination of the temperature field in an ice sheet are listed in Table 1. The two most important parameters are geothermal heat flow, affecting the basal temperature gradient, hence basal temperatures, and accumulation that affects vertical advection rates. Both parameters form the basis of a sensitivity analysis along two axes in parameter space. A first axis of 8 sensitivity experiments is given by uncertainties in GHF. Experiments are carried out with the data from Shapiro and Ritzwoller (2004) (SR), Fox-Maule et al. (2005) (FM), and Pollard et al. (2005) (P). This series is further extended with combinations of these data sets, i.e., (SR + FM)/2, (SR + P)/2, and (SR + FM + P)/3. Besides these, two spatially uniform GHF experiments were added, i.e. 42 and 54 mW m^{-2} . All datasets and their combinations were corrected for known temperature profiles and the occurrence of subglacial lakes with the method described above.

A second axis of 3 sensitivity experiments is given by uncertainties in accumulation rate. The standard experiment is based on the van de Berg et al. (2006) data. Two more experiments are added with anomalies of surface accumulation on a decadal timescale, i.e. for the period 1985–1994 and 1995–2004, based on Monaghan et al. (2006). These anomalies were chosen because they both show different spatial distributions on short time scales. Variability in accumulation over the last 20 years ranges between -20 and $+45\%$ of the current accumulation rate (Monaghan et al., 2006).

The complete sensitivity analysis encompasses of $8 \times 3 = 24$ experiments. Each model run takes about 26,000 CPU seconds on a HP XC Cluster Platform 4000 (HYDRA), composed of 2.4 GHz quad-cores. Due to the high resolution grid, each run requests 3–7 Gb memory space. The main advantage of such sensitivity runs is that that the analysis is not limited to just one ‘best guess’ model run, but that a statistical evaluation can be performed.

4.2. Basal temperatures

Fig. 3 displays the mean temperature field (mean of 24 experiments), its standard deviation and the likelihood that the ice sheet base is warm or cold. The mean surface of the grounded ice sheet at pressure melting point is 55%. Table 2 lists the percentage of the grounded ice sheet surface at pressure melting point for each of the experiments. Major differences in pressure melting distribution occur for perturbations in GHF, while perturbations in accumulation only have a limited effect on the surface subjected to pressure melting. The largest extension of pressure melting corresponds to FM data and its

combinations ($>60\%$), while the lowest extension (32%) is found for the spatially uniform GHF of 42 mW m^{-2} .

Standard deviations (Fig. 3B) are low ($<1^\circ\text{C}$) in zones where a priori temperature-dependent information is available. It covers to a large extent the central parts of the Antarctic ice sheet, where different types of subglacial lakes are present, i.e. the Lakes District, Recovery ice stream catchment, upstream of the Lambert Glacier catchment, and the Siple coast and its surroundings (West Antarctica). Nevertheless, areas where a priori information is lacking may exhibit low standard deviations as well. These are the coastal zones, upstream of grounding lines, where ice is relatively thick, surface elevation low, and where frictional heating due to faster ice transport along the major outlet glaciers keeps the base at pressure melting point, despite large horizontal advection rates associated with faster-moving ice.

Areas that are definitely cold generally show a larger standard deviation, mainly because of the intrinsic variability (for high temperatures, the pressure melting point can never be exceeded, while at low temperatures variations in both directions are possible). Definitely cold areas are associated with the presence of subglacial mountain ranges (thin ice), circumventing the Antarctic ice sheet, i.e. just upstream the coastal mountain ranges of Dronning Maud Land and the Transantarctic Mountains, but also the coastal areas of Wilkes and Enderby Land. In the central part of East Antarctica, cold ice is present across the Gamburtsev Subglacial Mountains (Dome Argus ice divide) and in the vicinity of Ridge B (between the warmer spots of Subglacial Lake Vostok and Sovetskaya/90°E Lakes). Because of the presence of the latter lake systems, the cold basal area associated with the Gamburtsev mountains is much smaller than in previous modeling studies (Siegert et al., 2005b; Huybrechts, 2006), since a higher heat flow is necessary to keep the lake area from freezing. Temperatures near Dome Argus are generally low (less than the truncated -10°C in Fig. 3A, with $\sigma \approx 4^\circ\text{C}$). The thin ice makes it unlikely that basal temperatures here would have been significantly different from these values over a glacial–interglacial cycle, as ice thickness changes in the center of the ice sheet are of the order of a few hundred meters (Huybrechts, 2002; Siegert et al., 2005b).

4.3. Basal melting

Mean basal melt rates and associated standard deviations are given in Fig. 4. Trends in melting rate patterns are similar to the basal temperature field. Highest melt rates ($>10 \text{ mm year}^{-1}$) are situated underneath ice shelves (where it is assumed that basal melt balances the accumulation rate; e.g. Holland and Jenkins, 1999). Highest melt rates underneath the grounded ice sheet are found in West Antarctica (Siple coast) and for all outlet glaciers of the ice sheet.

The mean melt rate underneath the grounded ice sheet according to all experiments is 5.3 mm year^{-1} . This leads to a total melt water volume of 65 Gt year^{-1} , a value much higher than previous estimates (Llubes et al., 2006). However, this is just a fraction of the total water volume of $22,000 \text{ km}^3$ that is estimated to be stored in the subglacial lake system (SALE Workshop Report, 2007) and much less than the amount of melt water produced under ice shelves. Here, our model predicts a total melt water volume of 435 Gt year^{-1} , a figure comparable to observed estimates of $540 \pm 218 \text{ Gt year}^{-1}$ (Church et al., 2001), although probably an underestimate. Basal melting of the grounded ice sheet represent 3% of the total accumulation based on the van de Berg et al. (2006) dataset.

4.4. Subglacial hydrology

A continuity equation for basal water flow is written as

$$\frac{\partial w}{\partial t} = -\nabla \cdot (\mathbf{v}_w w) + m, \quad (23)$$

Table 1

Major parameters and their degree of knowledge affecting the temperature field in sheets.

Parameter	Affects	Knowledge
GHF	$\frac{\partial T}{\partial z}$	Poor
a, v_s	Vertical advection	Good
T_s	Upper BC	Good
H	T_b	Improving
v_H	Horizontal advection	Modeled
v_b	Frictional heating	Modeled

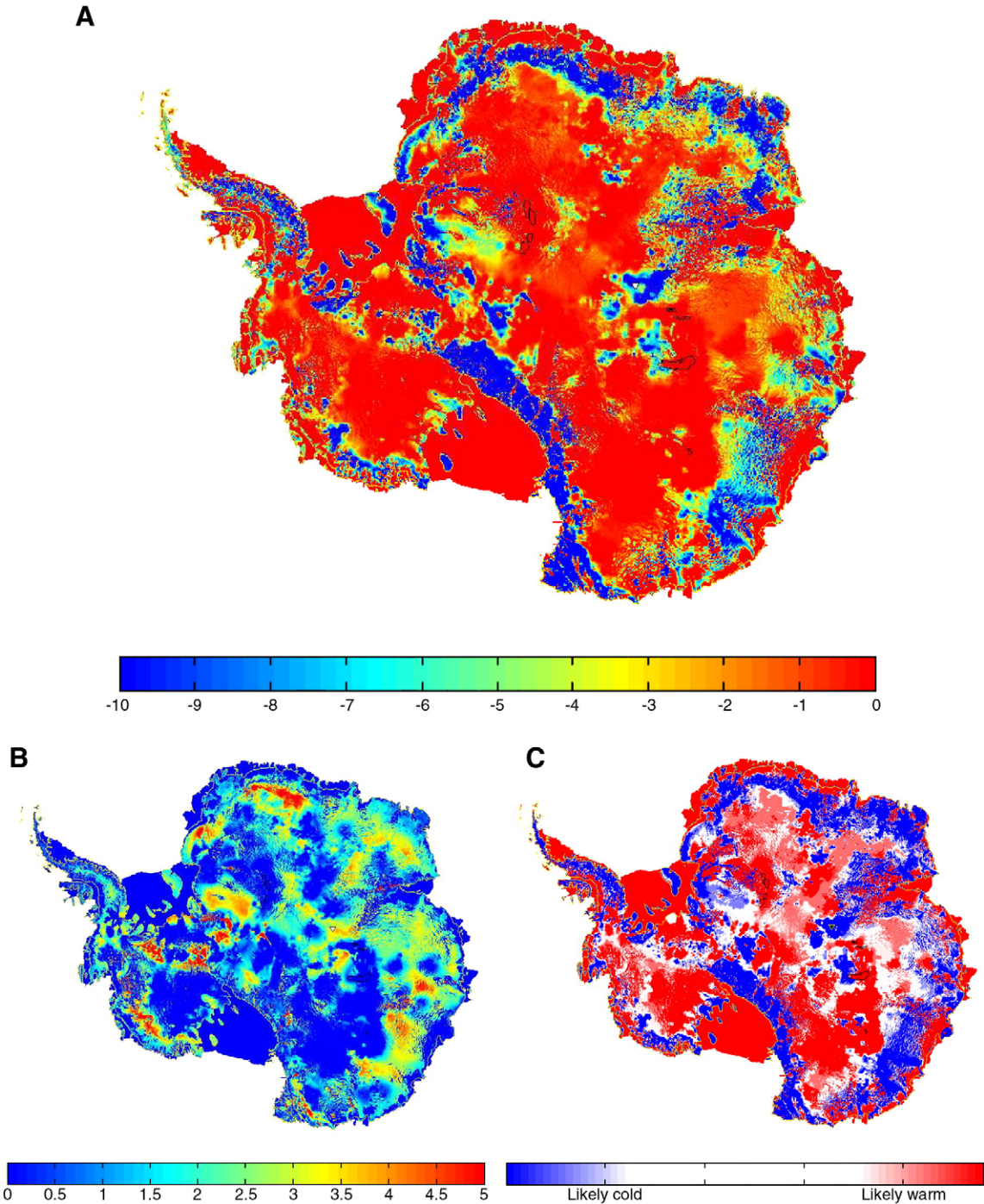


Fig. 3. (A) Mean basal temperature ($^{\circ}\text{C}$, corrected for pressure melting and truncated at $-10\text{ }^{\circ}\text{C}$); (B) standard deviation ($^{\circ}\text{C}$) for the 24 sensitivity experiments; and (C) likelihood of cold and warm bed (scale from 0 (cold-based in all experiments) to 24 (warm-based in all experiments)). The triangle shows the position of Dome Argus, where a new deep ice core drilling is planned.

where w is the thickness of the water layer (m) and \mathbf{v}_w the vertically integrated velocity of water in the layer (m year^{-1}). Considering steady-state conditions, the basal melting rate must balance the water flux divergence, or $m = \nabla \cdot (\mathbf{v}_w w)$ (Pattyn et al., 2005).

Subglacial water tends to move in the direction of decreasing hydraulic potential ϕ (Shreve, 1972). Assuming that basal water pressure is equal to the overlying ice pressure, the hydraulic potential gradient (or water pressure gradient) is written as $\nabla\phi = \rho_w g \nabla s + (\rho_w - \rho) g \nabla b$, where ρ_w is the subglacial water density. The steady-state basal water flux $\psi_w = (\mathbf{v}_w w)$ is obtained by integrating the basal melt rate m over the whole drainage basin, starting at the hydraulic head in the

direction of the hydraulic potential gradient $\nabla\phi$. This is also done with the computer scheme for balance flux calculations. Subglacial lakes are either end points or starting points in the subglacial routing algorithm, since they are natural water collectors in view of the hydraulic potential gradient. However, this only applies to the larger lakes that are definitely in hydrostatic equilibrium.

Since subglacial water flux is a function of ice sheet surface gradients and to a lesser extent bedrock gradients, its pattern (Fig. 5) is in agreement with the general pattern of ice flow. Therefore, maximum water flow concentrations are found in the major outlet glacier systems characterized by convergent ice flow, i.e. Lambert

Table 2

Percentage of the grounded ice sheet at pressure melting point for the 24 experiments (FM = Fox-Maule et al. (2005); SR = Shapiro and Ritzwoller (2004); P = Pollard et al. (2005); 42/54 = spatially uniform GHF (mW m^{-2}); Std a = van de Berg et al. (2006); Δa = decadal accumulation perturbation from Monaghan et al. (2006)).

	Std. a	Δa (1995–2004)	Δa (1985–1994)
FM	67.7	67.7	67.0
SR	54.4	54.6	53.3
FM + SR	63.2	63.1	62.1
P	55.5	55.3	54.7
P + SR	55.8	55.7	54.8
FM + P + SR	60.9	60.9	59.9
42	32.1	32.0	31.8
54	56.2	55.9	55.2
Mean	55.7	55.7	54.9

Glacier, Recovery Ice Streams, Byrd Glacier and Totten Glacier in East Antarctica; Siple Coast ice streams and Pine Island/Twaithes Glaciers in West Antarctica. Large subglacial lakes (displayed in Fig. 5) all lie at the head of the subglacial water system, such as Sovetskaya/90°E lake system, Subglacial Lake Vostok, and Subglacial Lake Concordia (Lakes District). The large subglacial lakes associated with the Recovery ice stream catchment are not lying at the head, but further downstream. They therefore receive a substantial amount of subglacial melt water from upstream, which makes them important water reservoirs of the East Antarctic ice sheet.

5. Discussion

5.1. Parameters affecting basal temperature

The interplay between GHF and accumulation rates is very sensitive, as high GHF increases basal temperatures, while high accumulation rates cool down the ice mass. This is illustrated in Fig. 6, displaying the minimum GHF needed to reach pressure melting point at the base of an ice sheet as a function of ice thickness and surface temperature, based on (20)–(22). Despite low surface temperatures (-50°C), pressure melting point is reached for relatively low values of GHF (40 mW m^{-2}), as long as the ice is near 4000 m thick and accumulation rates are small (0.05 m a^{-1}), which is rather typical for the interior parts of the East Antarctic ice sheet. For high accumulation rates (tenfold the previous value), one needs more than twice this GHF (90 mW m^{-2}) to reach melting point at the base.

An interesting feature according to Fig. 6 is that variations in ice thickness have less influence on the basal temperature field in regions

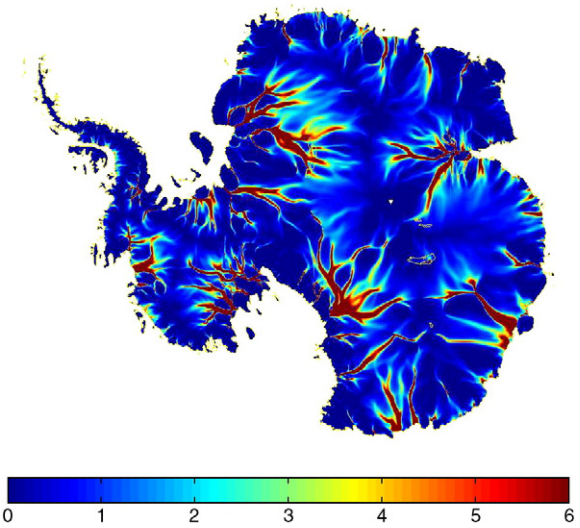


Fig. 5. Subglacial water flux ($10^3 \text{ m}^2 \text{ year}^{-1}$) based on the mean basal melt rate displayed in Fig. 4A. Values are truncated at $6 \times 10^3 \text{ m}^2 \text{ year}^{-1}$.

where the GHF is low (e.g. 40 mW m^{-2}) than in areas where the GHF is high (e.g. 100 mW m^{-2}). This is probably one of the reasons why the Lakes District is characterized by a rather constant (but low) GHF, despite significant ice thickness variability. On the contrary, the effect of ice thickness variability is much more pronounced in West Antarctica. However, since large parts of the WAIS are at pressure melting point, the variability is most pronounced in basal melting rates (Table 3).

5.2. Model assumptions

The quality of the results also depends on the assumptions made in the model. A major assumption is the steady-state condition for both the temperature field and ice thickness. Englacial temperatures react slowly to environmental changes and are therefore expected to still readjust to the glacial-interglacial transition. Ritz (1987) estimated that the impact of transient effects on the basal temperature could be up to 2 K (ice sheet base being colder than the steady-state one). This is the same order of magnitude as the standard deviation in the sensitivity experiment. However, during the last glacial period, surface temperatures were lower by 5–10 K, but ice velocities and

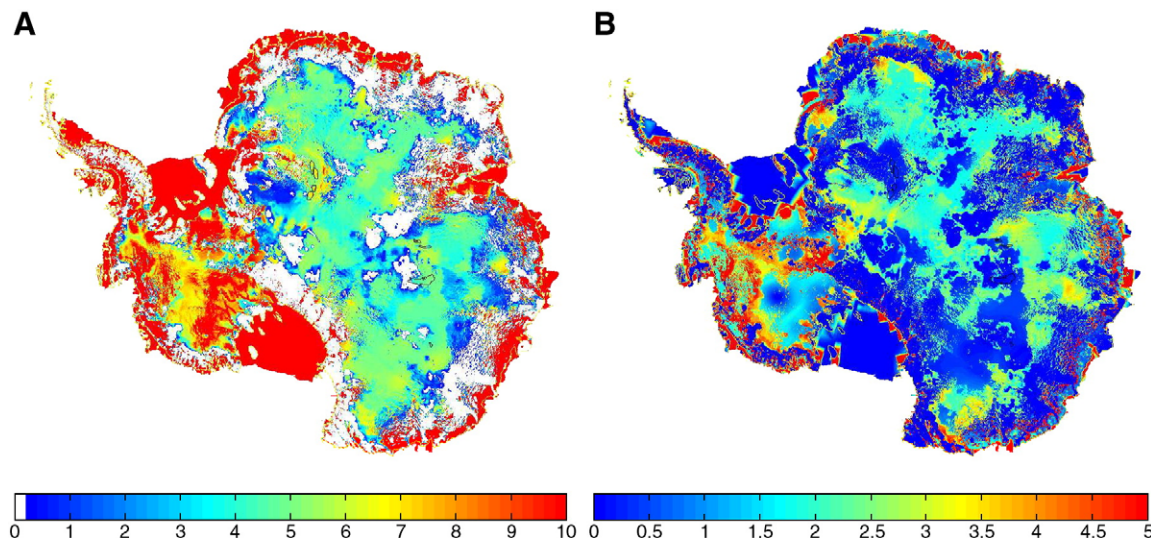


Fig. 4. (A) Mean basal melting rate (truncated at 10 mm year^{-1}) and (B) standard deviation (mm year^{-1}) for the 24 sensitivity experiments.

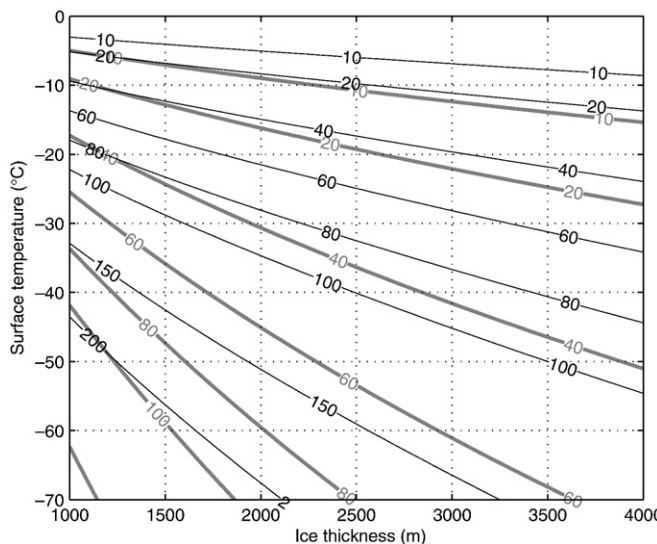


Fig. 6. Minimum GHF needed to reach pressure melting point as a function of ice thickness and surface temperature. A high vertical advection rate ($a = 0.5 \text{ m year}^{-1}$) is shown in a solid line, a low advection rate ($a = 0.05 \text{ m year}^{-1}$) in a dashed line.

accumulation rates were also lower, reducing the advection rates (both horizontal and vertical), hence reducing cooling of the basal layers.

In this study we deliberately refrained from the dynamical approach. The main reason is that ice thickness variations cannot be decoupled from the temperature field variations. Forcing the model over a number of glacial-interglacial cycles by the climatic record until present may yield a realistic ice sheet temperature field because of the inclusion of transient effects (Huybrechts, 2002), the modeled ice sheet surface topography may differ quite a lot from present-day observed topography by several hundreds of meters, which has a major impact on basal temperatures. Furthermore, it hampers the fitting to measured borehole temperatures. In view of the uncertainties on the other parameters (GHF, accumulation, ice thickness), the likelihood distribution of warm and cold areas in the ice sheet (Fig. 3C) is unlikely to be affected by this approach.

The quality of the model is also influenced by the data quality. Although the BEDMAP data base was updated with recently acquired data, there remain large sections where data gaps exist, such as the Gamburtsev Subglacial Mountains. Recent observations show that the ice sheet in this area overlies a classic Alpine topography with pre-existing river valleys overdeepened by valley glaciers (Bo et al., 2009). This particular area has relative low basal temperatures according to the model calculations, primarily due to the small ice thickness. Better constraints on the basal topography will probably reveal a more

Table 3

Total basal melt rate (Gt year^{-1}) underneath the grounded ice sheet for the 24 experiments (legend as in Table 2).

	Std. a	Δa (1995–2004)	Δa (1985–1994)
FM	79.3	78.0	77.8
SR	66.9	65.7	65.3
FM + SR	73.7	72.3	71.9
P	63.0	61.5	61.5
P + SR	65.1	63.7	63.5
FM + P + SR	69.8	68.5	68.2
42	41.0	39.7	39.9
54	61.4	59.9	59.8
Mean	65.0	63.7	63.5

complex pattern of basal temperatures, with higher values in the deeper parts covering the glacial valleys. Local variations in basal topography are thus essential in determining with sufficient detail basal temperature characteristics, for instance in preparation of drilling for old ice in Antarctica. For such studies, even a 5 km resolution grid will not be sufficient to capture the detail that is necessary.

5.3. Effect on basal ice age

Several deep ice core drillings have been carried out in the central parts of Antarctica. Of all deep ice cores, the EPICA Dome C ice reaches furthest down in time, approximately 800,000 years BP in a low accumulation area. However, at the bottom basal ice layers are presumed to be at pressure melting point. Other deep ice cores reached pressure melting point as well, such as EPICA DML and Dome Fuji, due to the increased insulation in regions of thick ice. However, when accumulation rates are too low, the resolution at depth is not resolved anymore. Therefore, the occurrence of the oldest ice is a sensitive interplay between ice thickness and accumulation rate, preferably in low GHF areas.

Although the age of the ice sheet depends on the accumulation history over glacial-interglacial periods, an age calculation of the ice sheet was performed anyway, not for the purpose of establishing a correct age-depth relationship everywhere in the ice sheet, but to estimate effects of our sensitivity analysis on the age of the deeper layers. Ice sheet age is written as an advection equation with a small diffusion term added in order to stabilize the numerical solution (Huybrechts, 1994; Greve, 1997):

$$\frac{\partial A}{\partial t} = \frac{\partial A}{\partial \zeta} \left(\frac{v_\zeta}{H} - v_x a_x - v_y a_y \right) + D_{\text{art}} - v_x \frac{\partial A}{\partial x} - v_y \frac{\partial A}{\partial y}, \quad (24)$$

where A is the ice age (year) and D_{art} a constant diffusion term ($2 \times 10^{-2} \text{ m}^2 \text{ year}^{-1}$). The equation was numerically solved for a period of 10^6 years under constant conditions of ice-flow field, accumulation and melt rates. Obviously, areas where older ice is found are those where no melting occurs (Fig. 7A). The standard deviation for the areas that – according to the sensitivity experiments – are always cold-based, is therefore low (Fig. 7B). However, for other areas the variation in basal melt rate is large enough to have standard deviations of 250 to 500,000 years, which is a very significant variation. Largest standard deviations occur in areas where ice is thickest and a small variation in basal melt rate significantly alters the age of the bottom ice layers.

6. Conclusions

Understanding the dynamics of polar ice sheets demands a better knowledge of subglacial conditions and interactions. Numerous studies have tried to determine basal conditions of the Antarctic ice sheet through dynamical thermomechanical modeling, thereby assuming either a spatially uniform geothermal heat flux or distributed datasets (Hansen and Greve, 1996; Ritz et al., 2001; Huybrechts, 2002; Pollard et al., 2005; Siegert et al., 2005b; Huybrechts, 2006; Llubes et al., 2006). However, improved basal temperature estimates should be in accord with observed temperature profiles – obtained from deep ice cores – and observed zones of melt water production, such as subglacial lakes. Recent studies found more than 280 subglacial lakes prevalent underneath the Antarctic ice sheet (Siegert et al., 2005a; Carter et al., 2007; Popov and Maslov, 2007; Smith et al., 2009). Most of these lakes are situated close to ice divides, but actively draining lakes are distributed under or at the head of ice streams (Bell et al., 2007; Fricker et al., 2007; Stearns et al.,

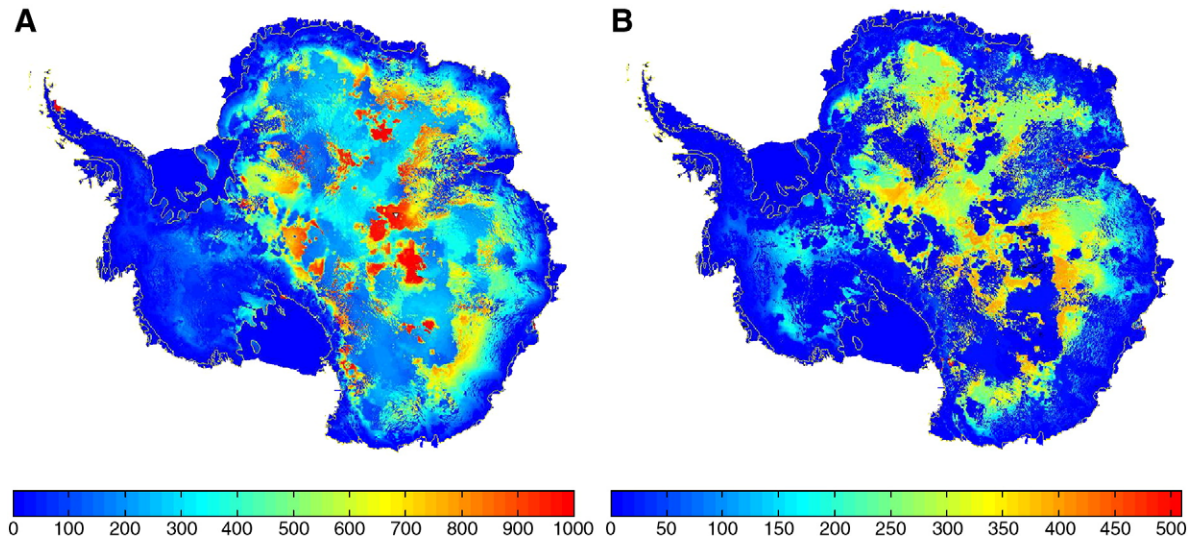


Fig. 7. (A) Mean ice age at 98% depth (10^3 year) and (B) standard deviation (10^3 years) for the 24 sensitivity experiments.

2008) and in faster ice-flow regions, such as West Antarctica (Smith et al., 2009).

In this paper, such a priori information was integrated in an ice sheet model, by a simple assimilation technique. The steady-state temperature field is calculated with a numerical ice sheet model. The velocity field is obtained from balance velocities, regionally enhanced with an ice stream model to correct for ice flow across large subglacial lakes (Pattyn et al., 2004). The a priori information concerning subglacial lake distribution and known vertical temperature profiles is used to correct several datasets of geothermal heat flow (GHF).

From the sensitivity experiments, carried out for perturbations in surface accumulation and GHF (different datasets and their combinations), it seems that 55% of the grounded part of the Antarctic ice sheet is at pressure melting point. Calculated basal melt rates are approximately 65 Gt year^{-1} , which is 3% of the total surface accumulation. The coldest spots (where the basal ice never reaches pressure melting point) is found in areas where ice is thinnest, i.e. across subglacial mountains (such as Gamburtsev Subglacial Mountains), and upstream of mountain ranges bordering the continent (Transantarctic Mountains, Dronning Maud land, ...).

Although these sensitivity experiments exhibit small variations in basal melt rates, the impact on the ice age of the basal layers is quite important. In areas that are characterized by relatively low melt rates, this may lead to standard deviations up to 50% (in a model run over a period of 10^6 years).

Finally, based on the mean melt basal melt rates, the steady-state basal water flux underneath the ice sheet was calculated with a balance flux model using the hydraulic potential gradient as a guidance. As expected, subglacial water flow concentrates underneath the large outlet glaciers of Antarctica. The larger subglacial lakes are perched at the head of these subglacial water systems. An exception, however, is the lake system of the Recovery Ice Stream Catchment (Bell et al., 2007), that receives a substantial amount of subglacial melt water from the upstream catchment.

Acknowledgments

This paper forms a contribution to the Belgian Research Programme on the Antarctic (Belgian Federal Science Policy Office), project nr. SD/CA/02 ‘Antarctic Subglacial Processes and Interactions (ASPI).’ I should like to thank J. Bamber, S. Fujita, J. MacGregor, K. Matsuoka, A. Monaghan, F. Pareninin, M. Studinger, M. van den Broeke and T. van Ommen for kindly providing the different datasets.

References

- Alley, R.B., Fahnestock, M., Joughin, I., 2008. Understanding glacier flow in changing times. *Science* 322, 1061–1062.
- Augustin, L., Motoyama, H., Wilhelms, F., Johnson, S., Hansen, S., Talalay, P., Vasiliev, N., 2007. Drilling comparison in ‘warm ice’ and drill design comparison. *Ann. Glaciol.* 47, 73–78.
- Bamber, J.L., Gomez-Dans, J.L., Griggs, J.A., 2009. A new 1 km digital elevation model of the Antarctic derived from combined satellite radar and laser data – part 1: data and methods. *Cryosphere* 3 (1), 101–111.
- Bell, R.E., 2008. The role of subglacial water in ice-sheet mass balance. *Nat. Geosci.* 1, 297–304.
- Bell, R.E., Studinger, M., Fahnestock, C.A.S.M.A., Joughin, I., 2007. Large subglacial lakes in East Antarctica at the onset of fast-flowing ice streams. *Nature* 445. doi:[10.1038/nature05554](https://doi.org/10.1038/nature05554).
- Bell, R.E., Studinger, M., Fahnestock, M.A., Shuman, C.A., 2006. Tectonically controlled subglacial lakes on the flanks of the Gamburtsev Subglacial Mountains, East Antarctica. *Geophys. Res. Lett.* 33, L02504. doi:[10.1029/2005GL025207](https://doi.org/10.1029/2005GL025207).
- Bindschadler, R., Bamber, J., Anandakrishnan, S., 2001. Onset of streaming flow in the Siple Coast region, West Antarctica. In: Alley, R., Bindschadler, R. (Eds.), *The West Antarctic Ice Sheet: Behavior and Environment: Vol. 77 of Antarct. Res. Ser.* AGU, Washington D.C., pp. 123–136.
- Bo, S., Siegert, M.J., Mudd, S.M., Sugden, D., Fujita, S., Xiangbin, C., Yunyun, J., Xueyuan, T., Yuansheng, L., 2009. The Gamburtsev Mountains and the origin and early evolution of the Antarctic Ice Sheet. *Nature* 459, 690–693.
- Budd, W.F., Warner, R.C., 1996. A computer scheme for rapid calculations of balance-flux distributions. *Ann. Glaciol.* 23, 21–27.
- Carter, S.P., Blankenship, D.D., Peters, M.F., Young, D.A., Holt, J.W., Morse, D.L., 2007. Radar-based subglacial lake classification in Antarctica. *Geochem. Geophys. Geosyst.* 8 (3), Q03016. doi:[10.1029/2006GC001408](https://doi.org/10.1029/2006GC001408).
- Christoffersen, P., Tulaczyk, S., 2003. Response of subglacial sediments to basal freezing. 1. Theory and comparison to observations from beneath the West Antarctic Ice Sheet. *J. Geophys. Res.* 108 (B4). doi:[10.1029/2002JB001935](https://doi.org/10.1029/2002JB001935).
- Church, J.A., Gregory, J.M., Huybrechts, P., Kuhn, M., Lambeck, K., Nhuan, M.T., Qin, Q., Woodworth, P.L., 2001. Changes in sea level. In: Houghton, J., Ding, Y., Griggs, D., Noguer, M., van der Linden, P., Dai, X., Maskell, K., Johnson, C. (Eds.), *Climate Change 2001: The Scientific Basis. Contribution of Working Group I to the Third Assessment Report of the International Panel on Climate Change*. Cambridge University Press, pp. 641–693. Cambridge, United Kingdom and New York, NY, USA.
- Dahl-Jensen, D., Morgan, V.L., Elcheikh, A., 1999. Monte Carlo inverse modelling of the Law Dome (Antarctica) temperature profile. *Ann. Glaciol.* 29, 145–150.
- Drewry, D.J., 1983. *Antarctic Glaciological and Geophysical Folio*. Scott Polar Research Institute, Cambridge.
- Fox-Maule, C., Purucker, M.E., Olsen, N., Mosegaard, K., 2005. Heat flux anomalies in Antarctica revealed by satellite magnetic data. *Science* 309, 464–467.
- Fricker, H.A., Scambos, T., 2009. Connected subglacial lake activity on lower Mercer and Whillans Ice Streams, West Antarctica, 2003–2008. *J. Glaciol.* 55 (190), 303–315.
- Fricker, H.A., Scambos, T., Bindschadler, R., Padman, L., 2007. An active subglacial water system in West Antarctica mapped from space. *Science* 315 (1544). doi:[10.1126/science.1136897](https://doi.org/10.1126/science.1136897).
- Fricker, H.A., Warner, R., Allison, I., 2000. Mass balance of the Lambert Glacier–Amery Ice Shelf system, East Antarctica: a comparison of computed balance fluxes and measured fluxes. *J. Glaciol.* 46 (155), 561–570.
- Fujii, Y., Azuma, N., Tanaka, Y., Nakayama, M., Kameda, T., Shinbori, K., Katagiri, K., Fujita, S., Takahashi, A., Kawada, K., Motoyama, H., Narita, H., Kamiyama, K., Furukawa, T., Takahashi, S., Shoji, H., Enomoto, H., Sitoth, T., Miyahara, T., Naruse, R.,

- Hondoh, T., Shiraiwa, T., Yokoyama, K., Ageta, Y., Saito, T., Watanabe, O., 2002. Deep ice core drilling to 2503 m depth at Dome Fuji, Antarctica. *Mem. Natl Inst. Polar Res., Spec. Issue* 56, 103–116.
- Fujita, S., Maeno, H., Uratsuka, S., Furukawa, T., Mae, S., Fujii, Y., Watanabe, O., 1999. Nature of radio echo layering in the Antarctic ice sheet detected by a two-frequency experiment. *J. Geophys. Res.* 104 (B6), 13,013–13,024.
- Gow, A.J., Ueda, H.T., Garfield, D.E., 1968. Antarctic ice sheet – preliminary results of first core hole to bedrock. *Science* 161 (3845), 1011–1013.
- Greve, R., 1997. Large-scale ice-sheet modelling as a means of dating deep ice cores in Greenland. *J. Glaciol.* 43 (144), 307–310.
- Hansen, I., Greve, R., 1996. Polythermal modelling of steady states of the Antarctic ice sheet in comparison with the real world. *Ann. Glaciol.* 23, 382–387.
- Hindmarsh, R.C.A., 1999. On the numerical computation of temperature in an ice sheet. *J. Glaciol.* 45 (151), 568–574.
- Hindmarsh, R.C.A., 2006. The role of membrane-like stresses in determining the stability and sensitivity of the Antarctic ice sheets: back pressure and grounding line motion. *Philos. Trans. R. Soc. A* 364, 1733–1767.
- Hindmarsh, R.C.A., Le Meur, E., 2001. Dynamical processes involved in the retreat of marine ice sheets. *J. Glaciol.* 47 (157), 271–282.
- Hindmarsh, R.C.A., Leysinger Vieli, G.J.M.C., Parrenin, F., 2009. A large-scale numerical model for computing isochrone geometry. *Ann. Glaciol.* 50 (51), 130–140.
- Holland, D.M., Jenkins, A., 1999. Modeling thermodynamic ice–ocean interactions at the base of an ice shelf. *J. Phys. Oceanogr.* 29 (8), 1787–1800.
- Hondoh, T., Shoji, H., Watanabe, O., Salamatian, A.N., Lipenkov, V., 2002. Depth-age and temperature prediction at Dome Fuji Station, East Antarctica. *Ann. Glaciol.* 35, 384–390.
- Hutter, K., 1983. Theoretical Glaciology. Kluwer Academic Publishers, Dordrecht.
- Huybrechts, P., 1992. The Antarctic ice sheet and environmental change: a three-dimensional modelling study. *Berichte für Polarforschung* 99, 1–241.
- Huybrechts, P., 1994. The present evolution of the Greenland ice sheet: an assessment by modelling. *Glob. Planet. Change* 9, 39–51.
- Huybrechts, P., 2002. Sea-level changes at the LGM from ice-dynamic reconstructions of the Greenland and Antarctic ice sheets during the glacial cycles. *Quatern. Sci. Rev.* 21, 203–231.
- Huybrechts, P., 2006. Numerical modeling of ice sheets through time. In: Knight, P. (Ed.), *Glacier Science and Environmental Change*. Blackwell Publishing, Oxford, pp. 406–412.
- Huybrechts, P., Steinhage, D., Wilhelms, F., Bamber, J., 2000. Balance velocities and measured properties of the Antarctic ice sheet from a new compilation of gridded data for modelling. *Ann. Glaciol.* 30, 52–60.
- Joughin, I.R., Tulaczyk, S., Bamber, J.L., Blankenship, D., Holt, J.W., Scambos, T., Vaughan, D.G., 2009. Basal conditions for Pine Island and Thwaites Glaciers, West Antarctica, determined using satellite and airborne data. *J. Glaciol.* 55 (190), 245–257.
- Kamb, B., Echelmeyer, K.A., 1986. Stress-gradient coupling in glacier flow: 1. Longitudinal averaging of the influence of ice thickness and surface slope. *J. Glaciol.* 32 (111), 267–298.
- Le Brocq, A.M., Payne, A.J., Siegert, M.J., 2006. West Antarctic balance calculations: impact of flux-routing algorithm, smoothing algorithm and topography. *Comput. Geosci.* 32, 1780–1795.
- Liu, H.X., Jezek, K.C., Li, B.Y., 1999. Development of an Antarctic digital elevation model by integrating cartographic and remotely sensed data: a geographic information system based approach. *J. Geophys. Res.* 104 (B10), 23,199–23,213.
- Llubes, M., Lanseau, C., Rémy, F., 2006. Relations between basal condition, subglacial hydrological networks and geothermal flux in Antarctica. *Earth Planet. Sci. Lett.* 241, 655–662.
- Lythe, M.B., Vaughan, D.G., 2001. BEDMAP: a new ice thickness and subglacial topographic model of Antarctica. *J. Geophys. Res.* 106 (B6), 11,335–11,351.
- MacAyeal, D.R., 1989. Large-scale ice flow over a viscous basal sediment: theory and application to Ice Stream B, Antarctica. *J. Geophys. Res.* 94 (B4), 4071–4087.
- MacGregor, J.A., Matsuoka, K., Koutnik, M.R., Waddington, E.D., Studinger, M., Winebrenner, D.P., 2009. Millennially averaged accumulation rates for the Vostok Subglacial Lake region inferred from deep internal layers. *Ann. Glaciol.* 50 (51), 25–34.
- MacGregor, J.A., Winebrenner, D.P., Conway, H., Matsuoka, K., Mayewski, P.A., Clow, G.D., 2007. Modeling englacial radar attenuation at Siple Dome, West Antarctica, using ice chemistry and temperature data. *J. Geophys. Res.* 112, F03008. doi:10.1029/2006JF000717.
- Monaghan, A.J., Bromwich, D.H., Fogt, R.L., Wang, S.H., Mayewski, P.A., Dixon, D., Ekyakin, A., Frezzotti, M., Goodwin, I., Isaksson, E., Kaspari, S.D., Morgan, V.I., Oerter, H., Van Ommen, T.D., van der Veen, C.J., Wen, J., 2006. Insignificant change in Antarctic snowfall since the International Geophysical Year. *Science* 313, 827–831.
- Parrenin, F., Dreyfus, G., Durand, G., Fujita, S., Gagliardini, O., Gillet, F., Jouzel, J., Kawamura, K., Lhomme, N., Masson-Delmotte, V., Ritz, C., Schwander, J., Shoji, H., Uemura, R., Watanabe, O., Yoshida, N., 2007. 1-D-ice flow modelling at EPICA Dome C and Dome Fuji, East Antarctica. *Clim. Past* 3, 243–259.
- Parrenin, F., Remy, F., Ritz, C., Siegert, M., Jouzel, J., 2004. New modelling of the Vostok ice flow line and implication for the glaciological chronology of the Vostok ice core. *J. Geophys. Res.* 109, D20102. doi:10.1029/2004JD004561.
- Pattyn, F., 2003. A new 3D higher-order thermomechanical ice-sheet model: basic sensitivity, ice-stream development and ice flow across subglacial lakes. *J. Geophys. Res.* 108 (B8, 2382). doi:10.1029/2002JB002329.
- Pattyn, F., 2008. Investigating the stability of subglacial lakes with a full Stokes ice-sheet model. *J. Glaciol.* 54 (185), 353–361.
- Pattyn, F., De Smedt, B., Souchez, R., 2004. Influence of subglacial Lake Vostok on the regional ice dynamics of the Antarctic ice sheet: a model study. *J. Glaciol.* 50 (171), 583–589.
- Pattyn, F., De Brabander, S., Huyghe, A., 2005. Basal and thermal control mechanisms of the Ragnhild glaciers, East Antarctica. *Ann. Glaciol.* 40, 225–231.
- Pattyn, F., Huyghe, A., De Brabander, S., De Smedt, B., 2006. Role of transition zones in marine ice sheet dynamics. *J. Geophys. Res.* 111 (F02004). doi:10.1029/2005F000394.
- Peters, M.E., Blankenship, D.D., Morse, D.L., 2005. Analysis techniques for coherent airborne radar sounding: application to West Antarctic ice streams. *J. Geophys. Res.* 110 (B06303). doi:10.1029/2004JB003222.
- Pollard, D., DeConto, R.M., Nyblade, A.A., 2005. Sensitivity of Cenozoic Antarctic ice sheet variations to geothermal heat flux. *Glob. Planet. Change* 49, 63–74.
- Popov, S.V., Masolov, V.N., 2007. Forty-seven new subglacial lakes in the 0–110° sector of East Antarctica. *J. Glaciol.* 53 (181), 289–297.
- Pounder, E.R., 1965. Physics of Ice. Pergamon Press, Oxford.
- Price, P.B., Nagornov, O.V., Bay, R., Chirkin, D., He, Y., Miocinovic, P., Richards, A., Woschnagg, K., Koci, B., Zagorodnov, V., 2002. Temperature profile for glacial ice at the South Pole: implications for life in a nearby subglacial lake. *Proc. Natl. Acad. Sci.* 99 (12), 7844–7847.
- Ritz, C., 1987. Time dependent boundary conditions for calculation of temperature fields in ice sheets. *IAHS Publ.* 170, 207–216.
- Ritz, C., Rommelaeer, V., Dumas, C., 2001. Modeling the evolution of the Antarctic ice sheet over the last 42000 years: implications for altitude changes in the Vostok region. *J. Geophys. Res.* 106 (D23), 31,943–31,964.
- Ruth, U., Barnola, J., Beer, J., Bigler, M., Blunier, T., Castellano, E., Fischer, H., Fundel, F., Huybrechts, P., Kaufmann, P., Kipfstuhl, S., Lambrecht, A., Morganti, A., Oerter, H., Parrenin, F., Rybak, O., Severi, M., Udisti, R., Wilhelms, F., Wolff, E., 2007. “EDML1”: a chronology for the EPICA deep ice core from Dronning Maud Land, Antarctica, over the last 150,000 years. *Clim. Past* 3, 475–484.
- Salamatin, A.N., Lipenkov, V.Y., Blinov, K.V., 1994. Vostok (Antarctica) climate record time-scale deduced from the analysis of a borehole-temperature profile. *Ann. Glaciol.* 20, 207–214.
- SALE Workshop Report, 2007. Subglacial Antarctic Lake Environments (SALE) in the International Polar Year 2007–2008. Advanced Science and Technology Planning Workshop, 24–26 April 2006, Grenoble France.
- Shapiro, N.M., Ritzwoller, M.H., 2004. Inferring surface heat flux distributions guided by a global seismic model: particular application to Antarctica. *Earth Planet. Sci. Lett.* 223, 213–224.
- Shreve, R.L., 1972. Movement of water in glaciers. *J. Glaciol.* 11 (62), 205–214.
- Siegert, M.J., 2000. Antarctic subglacial lakes. *Earth-Sci. Rev.* 50, 29–50.
- Siegert, M.J., Carter, S., Tobacco, I., Popov, S., Blankenship, D., 2005a. A revised inventory of Antarctic subglacial lakes. *Antarct. Sci.* 17 (3), 453–460.
- Siegert, M.J., Taylor, J., Payne, A.J., 2005b. Spectral roughness of subglacial topography and implications for former ice-sheet dynamics in East Antarctica. *Glob. Planet. Change* 45, 249–263.
- Smith, B.E., Fricker, H.A., Joughin, I.R., Tulaczyk, S., 2009. An inventory of active subglacial lakes in Antarctica detected by ICESat (2003–2008). *J. Glaciol.* 55 (192), 573–595.
- Stearns, L.A., Smith, B.A., Hamilton, G.S., 2008. Increased flow speed on a large East Antarctic outlet glacier caused by subglacial floods. *Nat. Geosci.* 1, 827–831.
- Studinger, M., Bell, R.E., Karner, G.D., Tikku, A.A., Holt, J.W., Morse, D.L., Richter, T.G., Kempf, S.D., Peters, M.E., Blankenship, D.D., Sweeney, R.E., Rystrom, V.L., 2003. Ice cover, landscape setting, and geological framework of Lake Vostok, East Antarctica. *Earth Planet. Sci. Lett.* 205, 195–210.
- van de Berg, W.J., van den Broeke, M.R., Reijmer, C.H., van Meijgaard, E., 2006. Reassessment of the Antarctic surface mass balance using calibrated output of a regional atmospheric climate model. *J. Geophys. Res.* 111 (D11104). doi:10.1029/2005JD006495.
- van den Broeke, M.R., 2008. Depth and density of the Antarctic firn layer. *Arct. Antarct. Alp. Res.* 40 (2), 432–438.
- van den Broeke, M.R., van de Berg, W.J., van Meijgaard, E., 2006. Snowfall in coastal West Antarctica much greater than previously assumed. *Geophys. Res. Letters* 33 (L02505). doi:10.1029/2005GL025239.
- van Ommen, T.D., Morgan, V.I., Jacka, T.H., Woon, S., Elcheikh, A., 1999. Near-surface temperatures in the Dome Summit South (Law Dome, East Antarctica) borehole. *Ann. Glaciol.* 29, 141–144.
- Watanabe, O., Jouzel, J., Johnsen, S., Parrenin, F., Shoji, H., Yoshida, N., 2003. Homogeneous climate variability across East Antarctica over the past three glacial cycles. *Nature* 422, 509–512.
- Zotikov, I., 1963. Bottom melting in the central zone of the ice shield of the Antarctic continent and its influence upon the present balance of the ice mass. *Bull. Int. Assoc. Scient. Hydrol.* 8 (1), 36.